Hybrid orthogonal junctions: wideband plasmonic slot-silicon waveguide couplers

Benedict Lau, Mohamed A. Swillam, and Amr S. Helmy*

Edward S. Rogers Sr. Department of Electrical and Computer Engineering, University of Toronto, Toronto, M5S 3G4, Canada
**a.helmy@utoronto.ca,*

Abstract: In this paper, novel ultra compact and ultra wide band couplers between silicon and plasmonic slot waveguides are analyzed, characterized, and fabricated. This novel coupling scheme is fabricated using silicon on insulator platform. An orthogonal junction configuration is designed to provide non-resonate wideband coupling from a 400 nm silicon waveguide to 50-nm wide air-filled plasmonic slot. The 1 μm wide full-width half-max coupling spectrum can theoretically reach high peak of 70% coupling to the plasmonic slot centered around the 1550 nm wavelength. This center wavelength can be controlled by varying the silicon waveguide width. Theoretical analysis is in good agreement with FDTD simulated results, and experimental results. The fabrication procedure is also presented and discussed.

OCIS codes: (240.6680) Surface plasmons; (250.5403) Plasmonics; (160.3918) Metamaterials; (130.2790) Guided waves; (280.4788) Optical sensing and sensors.

References and links

1. J. Homola, S. S. Yee, and G. Gauglitz, "Surface plasmon resonance sensors: review," Sens. Actuators B Chem. **54**(1-2), 3–15 (1999).
2. M. A. Swillam, and A. S. Helmy, "Analysis and applications of 3D rectangular metallic waveguides," Opt. Express **18**(19), 19831–19843 (2010).
3. J. Homola, "Present and future of surface plasmon resonance biosensors," Anal. Bioanal. Chem. **377**(3), 528–539 (2003).
4. S. A. Maier, "Plasmonic field enhancement and SERS in the effective mode volume picture," Opt. Express **14**(5), 1957–1964 (2006).
5. P. Berini, "Bulk and surface sensitivity of surface plasmon waveguide," N. J. Phys. **10**(10), 105010 (2008).
6. H. J. Caulfield, and S. Dolev, "Why future supercomputing requires optics," Nat. Photonics **4**(5), 261–263 (2010).
7. B. G. Lee, X. Chen, A. Biberman, X. Liu, I.-W. Hsieh, C.-Y. Chou, J. I. Dadap, F. Xia, W. M. J. Green, L. Sekaric, Y. A. Vlasov, R. M. Osgood, Jr., and K. Bergman, "Ultrahigh-bandwidth silicon photonic nanowire waveguides for on-chip networks," IEEE Photon. Technol. Lett. **20**(6), 398–400 (2008).
8. E. Feigenbaum, and M. Orenstein, "Modeling of Complementary (Void) Plasmon Waveguiding," J. Lightwave Technol. **25**(9), 2547–2562 (2007).
9. L. Chen, J. Shakya, and M. Lipson, "Subwavelength confinement in an integrated metal slot waveguide on silicon," Opt. Lett. **31**(14), 2133–2135 (2006).
10. Z. Han, A. Y. Elezzabi, and V. Van, "Experimental realization of subwavelength plasmonic slot waveguides on a silicon platform," Opt. Lett. **35**(4), 502–504 (2010).
11. Z. Han, A. Elezzabi, and V. Van, "Wideband Y-splitter and aperture-assisted coupler based on sub-diffraction confined plasmonic slot waveguides," Appl. Phys. Lett. **96**(13), 131106 (2010).
12. G. Veronis, and S. Fan, "Modes of subwavelength plasmonic slotwaveguides," J. Lightwave Technol. **25**(9), 2511–2521 (2007).
13. G. Veronis, and S. Fan, "Bends and splitters in metal-dielectric-metal subwavelength plasmonic waveguides," Appl. Phys. Lett. **87**(13), 131102 (2005).
14. N. N. Feng, M. L. Brongersma, and L. Dal Negro, "Metal-dielectric slot waveguide structures for the propagation of surface plasmon polaritons at 1.55 μm," IEEE J. Quantum Electron. **43**(6), 479–485 (2007).
15. G. B. Hoffman, and R. M. Reano, "Vertical coupling between gap plasmon waveguides," Opt. Express **16**(17), 12677–12687 (2008).
16. G. Veronis, and S. H. Fan, "Theoretical investigation of compact couplers between dielectric slab waveguides and two-dimensional metal-dielectric-metal plasmonic waveguides," Opt. Express **15**(3), 1211–1221 (2007).
17. H. Raether, *Surface Plasmons on Smooth and Rough Surfaces and on Gratings*, (Springer-Verlag, Berlin, 1988).
18. F. D. T. D. Luemrical, Lumerical Solutions, Inc.http://www.lumerical.com

#136455 - $15.00 USD Received 11 Oct 2010; revised 22 Nov 2010; accepted 26 Nov 2010; published 8 Dec 2010

19. E. D. Palik, *Handbook of optical constants of solids*,(Academic press,1998).

1. Introduction

Surface plasmon polariton (SPP) waveguides have attracted much attention in the last decade due to the wealth of applications enabled by their unique ability to guide light at subwavelength scales. The ability to guide the optical field on the metal surface or between two metal surfaces provides distinctive and unique sensing capabilities for these waveguides. Thus, these SPP waveguides are exploited in many sensing and biosensng applications as they provide compactness and high sensitivity [1,2]. It has been utilized also to enhance the Raman signal in surface-enhanced Raman scattering (SERS) [3,4]. In addition, SPP waveguides are recently used as fluidic channels for surface and bulk biosensing using Mach-Zehnder interferometer configuration [5].

The nanometer-scale confinement makes the plasmonic waveguides good candidates also for on-chip optical interconnect that can interface with CMOS electronics. Replacing the conventional metallic wires with high bandwidth optical interconnects would allow buses to operate at speeds much faster than those being used in the current state-of-the-art integrated circuits (ICs) [6]. It has been shown that significant performance gains can be realized by utilizing an optical layer for global clock distribution at the top of an IC stack [7] but there is great potential at the transistor-level layers, where short local interconnects link up local circuit modules. If we can confine light into small cross-sectional dimensions on the order of tens of nanometers, while limiting the loss to allow for sufficient signal propagation lengths between these local modules, the optical network can replace metallic interconnects at all levels of an IC chip. This system would allow transistors to operate at their peak performances.

Numerous plasmonic waveguide configurations have been proposed for various applications [2,8]. Amongst them, the metal-insulator-metal (MIM) and insulator-metal-insulator (IMI) are the most widely studied. The plasmonic slot waveguide (PSW) can be considered a three-dimensional variation of the MIM, where a deeply subwavelength slot is surrounded by the metallic side walls along the horizontal direction, and embedded in dielectric materials along the vertical dimension.

This specific PSW has been recently fabricated using different approaches depending on the targeted applications [9,10]. For example, in [9] a 150 nm wide silicon (Si) waveguide is covered with gold to provide the strong guidance. This approach provides an easy technique for the PSW fabrication, however, it might be necessary to further miniaturize the slot dimensions. In addition, this configuration is not suitable for sensing as the slot is already occupied by the silicon. The design in [10] is also subject to similar limitations, where the 200 nm wide slot is filled with PMMA. Various designs of tapering structures are employed for the coupling from a silicon waveguide to the PSW [9,10]. The slot is often filled with a matching media to enhance the amount of the power coupled from the silicon waveguide media by minimizing the modal mismatch. The same platform has also been exploited to propose different plasmonic slot based components such as *y*-junction and couplers [11].

The PSW with air filling slot is considered the most suitable design for sensing and optical interconnects at the same time. Among all the other 2D waveguide configurations, PSW is considered as the most sensitive plasmonic waveguide structure for the filling media [5]. This design has been extensively modeled and theoretically investigated [7,12–16]. However, few experimental demonstrations exist [15]. This is mainly due to the demanding fabrication requirements of the structure especially when the slots are only a few tens of nanometers in width. The coupling mechanism for mode excitation also becomes a major challenge as one-order-of-magnitude larger dielectric waveguides are not naturally phase-matched to deeply subwavelength plasmonic slots to enable efficient coupling.

Here, we propose a novel technique for broadband coupling to and from a 50 nm wide air-filled PSW. Conventional silicon wire waveguide 340 nm tall and 400 nm wide are utilized as the access waveguides. Theoretical investigation and finite difference time domain (FDTD) simulations are carried out to verify the concept and explain the coupling mechanism in this

#136455 - $15.00 USD Received 11 Oct 2010; revised 22 Nov 2010; accepted 26 Nov 2010; published 8 Dec 2010

particular configuration. Different design parameters and their effect on the coupling mechanism are also studied. A prototype device based on a silicon on insulator (SOI) substrate is fabricated to provide good demonstration of this coupling platform. This novel coupling scheme provides a suitable platform that can be employed in optical interconnects applications. It also provides a novel scheme for nano-scale biosensing and SERS applications. Creating array of plasmonic slot waveguides with well defined access ports (silicon waveguides) using the proposed scheme can be also employed for highly sensitive, compact, integrated biosensors.

We start by briefly describing the theoretical analysis of the orthogonal coupling scheme in Section 2. The modeling and the FDTD simulations are given in Section 3. In Section 4, the fabrication details and measurements results are demonstrated and discussed. Finally, the conclusion is given in Section 5.

2. Hybrid orthogonal coupling

In general, the SPP mode has momentum mismatch with the plane wave or conventional waveguide modes. Thus, prism or Bragg gratings are mainly utilized for coupling from plane waves to the SPP mode on a single interface to compensate for this momentum mismatch [17] The plasmonic slot mode consists of two coupled SPP surface modes, confining the TM light in a few tens of nanometers, making it especially difficult to apply these standard coupling techniques to interface with the plasmonic waveguide with a practical coupling efficiency.

The weak coupling between the silicon waveguide and the PSW is mainly due to the significant mismatch in the momentum of the fundamental mode in each of them. There are two main reasons for the huge momentum mismatch; the first one is mainly due to the inherent difference in momentum between the SPP mode on any single interface and waveguide or plane waves which requires special coupling mechanism as mentioned earlier. The second is due to the slot dimension, which is usually one order of magnitude smaller than the conventional silicon waveguide. The combined mismatch can be demonstrated through the dispersion characteristics as shown in Fig. 1. In this figure, the propagation constant of the fundamental mode of the silicon waveguide, k_z, has much higher values than the one for the fundamental mode of the plasmonic slot, k_{SPP}, over the entire optical communication frequency band. Direct end-fire coupling between the two waveguide produces small coupling power and also may cause resonance effects, limiting the operation bandwidth.

The conventional approach for reducing the momentum mismatch is by using a tapered section, which reduces the lateral dimension of the Si waveguide. The tapered structure has been utilized in many different forms [9,10]. The main drawback for this approach is the requirement of long propagation section, which increases the overall dimension of the structure, the losses, and the complexity. Reducing the tapering section length may result in creating a standing wave inside the tapered section due to the impendence mismatch at the two ends of the taper [9]. This standing wave may cause resonance effects and hence reduces the coupling bandwidth and compromise the functionality of the waveguide.

Obtaining broadband coupling with minimum resonance effect is thus of prime importance. To fulfill these requirements, we propose a novel scheme based on orthogonal coupling by employing a 90° degree angle between the PSW and the Si waveguide as shown in Fig. 2. The orthogonal coupling scheme proposed in this paper provides an alternative solution for the momentum mismatch without the added tapers. This coupling scheme is based on matching the orthogonal momentum component of the silicon waveguide, k_x, with the PSW momentum component instead of the longitudinal component as in conventional schemes. As clear from Fig. 1, this k_x component has a small mismatch with the k_{SPP} over a large bandwidth. In order to exploit k_x in coupling the power to the plasmonic slot, this component has to be spatially aligned with the k_{SPP}. To achieve this condition, the two waveguides should be orthogonally coupled as shown in Fig. 2.

The k_x component of the Si waveguide shares the same value with k_{SPP} at a specific wavelength. At this wavelength the coupling is maximized. The intersection point can be tuned by varying the waveguide dimensions. This point is red shifted with the increase of the

#136455 - $15.00 USD Received 11 Oct 2010; revised 22 Nov 2010; accepted 26 Nov 2010; published 8 Dec 2010

Si waveguide width. In addition, the insignificant momentum mismatch obtained using this scheme allows for high coupling efficiencies over a wide bandwidth. This scheme also avoids any significant resonance effects when a cavity is formed, despite the large impendence mismatch between the two sections. These results are verified using FDTD simulation hereafter.

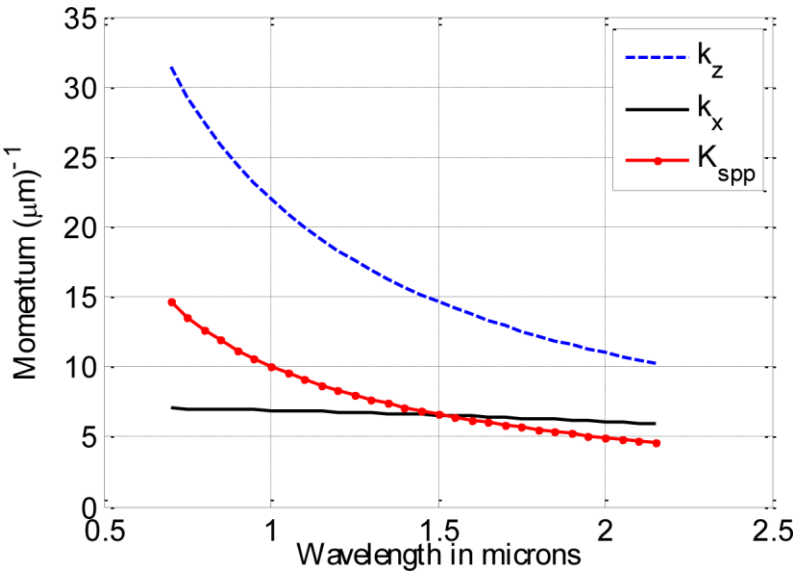

Fig. 1. The dispersion characteristics of the PSW and silicon waveguide. The PSW has a dimension of 50 nm gap and 340 height, silicon waveguide is 400 nm wide and 340 nm height.

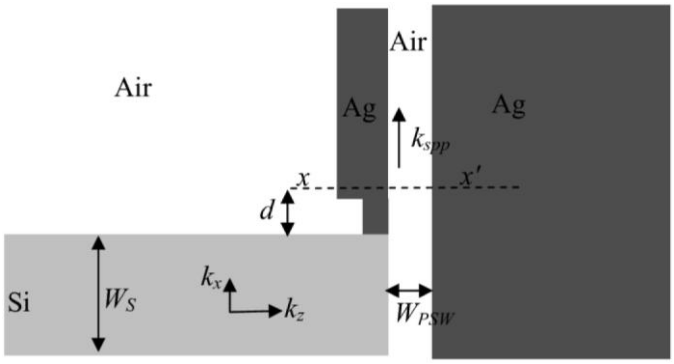

Fig. 2. Schematic diagram of the orthogonal coupling technique (top view).

#136455 - $15.00 USD Received 11 Oct 2010; revised 22 Nov 2010; accepted 26 Nov 2010; published 8 Dec 2010

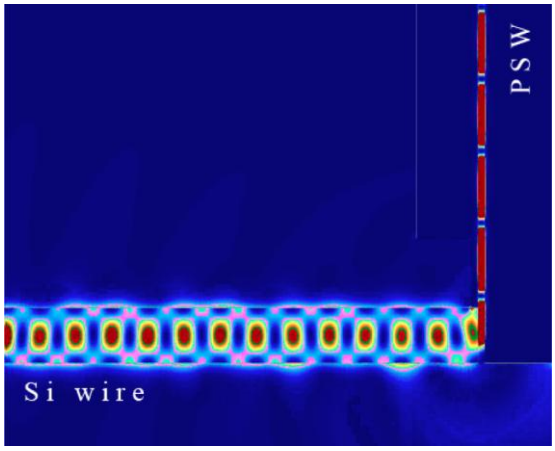

Fig. 3. Coupling from silicon waveguide to PSW upon 1550 nm continuous wave excitation. Bright spots generated by 2D FDTD depict the electric field intensities overlaying the structure in Fig. 2.

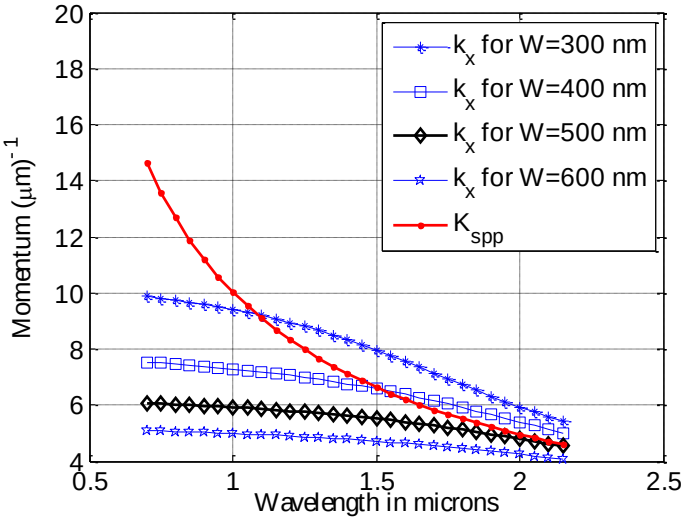

Fig. 4. The dispersion characteristics of the PSW and silicon waveguide for different for different width of the silicon waveguide.

3. Modeling and simulation

FDTD is exploited to simulate the broadband coupling from a Si waveguide to the PSW in this orthogonal configuration. The commercial software Lumerical FDTD [18] is employed and the effects of various parameters are analyzed. The following parameters are used to mesh the plasmonic section, which contains the smallest features and deserve special attention:

Cross-sectional width of slot: 2 nm wide cells

Cross-sectional height of slot: 5 nm wide cells

Propagation direction: 50 nm wide cells

#136455 - $15.00 USD Received 11 Oct 2010; revised 22 Nov 2010; accepted 26 Nov 2010; published 8 Dec 2010

Perfectly matched layer (PML) boundaries are utilized to terminate the computational domain. Figure 3 maps the electric field intensities upon continuous-wave excitation, which visually demonstrates the coupling mechanism in the orthogonal configuration shown in Fig. 2

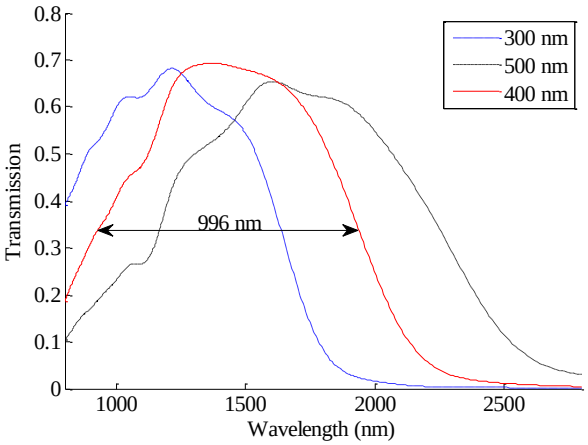

Fig. 5. Transmission spectra generated by 3D FDTD red shifting with increasing silicon waveguide widths.

For silver a numerical model based on high order polynomial fitting of the measured data [19] is exploited in dispersive FDTD [18].

To measure the transmission, a detector is placed at the cross-section of the PSW 10 nm away from the Si waveguide sidewall, labeled as *d* in Fig. 2. The normalized transmission is calculated such that the power flux through the detector is integrated and normalized with respect to the source power. The source is a Si waveguide mode source 1 μm away from the PSW, generating a short pulse that spans wavelengths from 800 nm to 2800 nm. Using this model, we can analyze the coupling efficiency of this orthogonal configuration.

For coupling from Si waveguide to PSW using the orthogonal configuration, the one order of magnitude size mismatch between the two sections no longer sets an upper bound to the Si waveguide width, as in the case of end-fire coupling, since the waveguide is directed towards the side of the PSW along its length. As expected from analytical studies, the transmission spectrum red shifts with increasing Si waveguide width. The momentum-matching analysis and FDTD results are shown in Figs. 4 and 5, respectively. We find that a 400 nm wide Si waveguide would provide a 996 nm wide 3 dB envelop centered near the 1550 nm wavelength.

Figure 6 shows that at 1550 nm, the peak coupling efficiency occurs for a Si waveguide about 430 nm in width and the coupling loss is about 30%. This design gives a 3 dB coupling spectrum about 1 μm wide. By also eliminating the upper bound in waveguide dimensions, we can use wide silicon waveguides for narrower plasmonic slots, producing a broadband transmission spectrum shifted above the silicon waveguide absorption wavelengths.

One of the key advantages of the PSW design is that it allows for access to the slot core, which means it may be filled with a material with a different refractive index than air. We have previously explained how various implementations of the PSW in the literature do not allow for accessing this slot. In this orthogonal coupling platform design and the fabrication process flow, the slot can be filled by spinning a polymer layer on the device surface. Hereafter, the effect of changing the refractive index of the slot region, *n*, on the coupling efficiency of the orthogonal coupling scheme is presented.

Figure 7 shows that the k_x and k_{SPP} mismatch increases with increasing slot index, *n*. This is undesirable as the coupling efficiency is expected to suffer. 3D FDTD is therefore employed to determine the additional losses for practical refractive indices between 1.0 to 2.0,

#136455 - $15.00 USD Received 11 Oct 2010; revised 22 Nov 2010; accepted 26 Nov 2010; published 8 Dec 2010

and the results are shown in Fig. 8. The effects appear to be a combination of the narrowing of the coupling band as well as higher coupling losses, but up to n = 1.5, the additional losses are

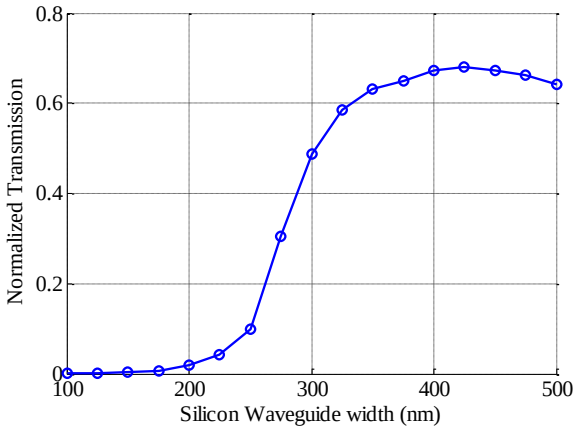

Fig. 6. Transmission vs. silicon waveguide width generated by 3D FDTD plotted at 1550 nm wavelength. The peak transmission reaches about 70% for a silicon waveguide 430 nm wide.

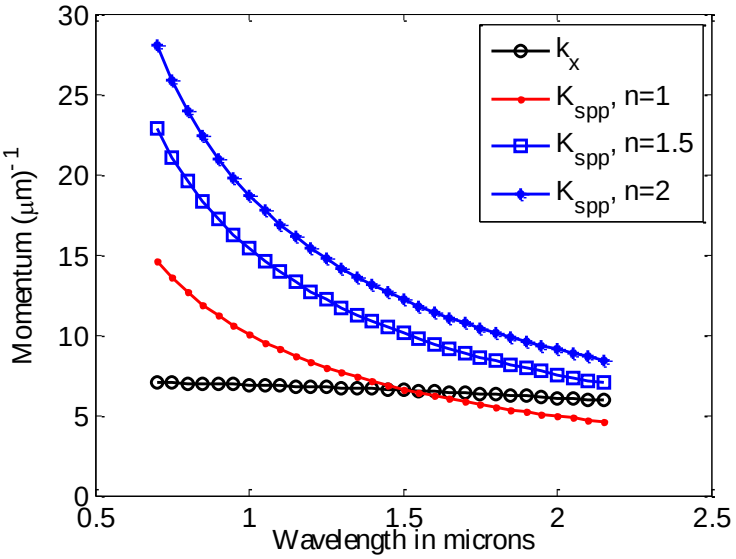

Fig. 7. The dispersion characteristics of the PSW and silicon waveguide for different refractive index of the filled material in the slot region.

insignificant. The momentum matching model does not take into account the effect of the field matching specially in the vertical direction.

In order to optically characterize the PSW losses and the orthogonal coupling scheme, the platform shown in Fig. 9 is designed. Because of the multi-sectioned design, cavities are formed that give rise to resonance effects. As with previous designs [16] the transmission becomes wavelength dependent for a given cavity length because of the effective index mismatched regions. This consequence may be undesirable for certain applications such as optical interconnects, where the lines carrying high bit-rate signals may be of different lengths.

#136455 - $15.00 USD Received 11 Oct 2010; revised 22 Nov 2010; accepted 26 Nov 2010; published 8 Dec 2010

In the end-fire (parallel) coupling configuration, 2D finite difference frequency domain (FDFD) simulations carried out at a 1550 nm wavelength have shown strong resonances as the cavity length is swept from 0 to 2000 nm [16]. These results are reproduced using 2D FDTD and are shown in Fig. 10. The results for the orthogonal configuration are shown in the same figure and the resonance depths are much smaller, which means the orthogonal scheme has a coupling spectrum that is only weakly wavelength dependent in comparison. The reason

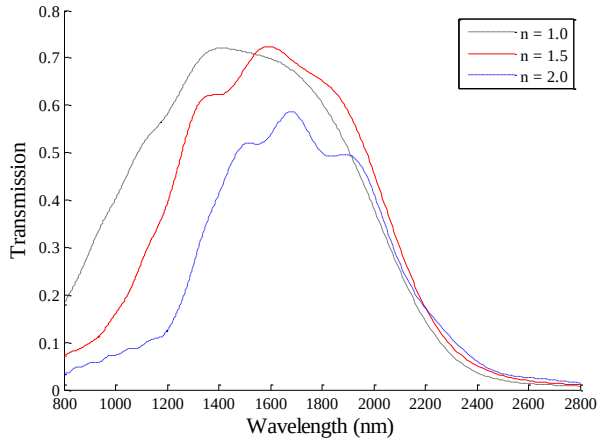

Fig. 8. Transmission spectra generated by 3D FDTD attenuated as *n* is increased from 1.0 to 2.0.

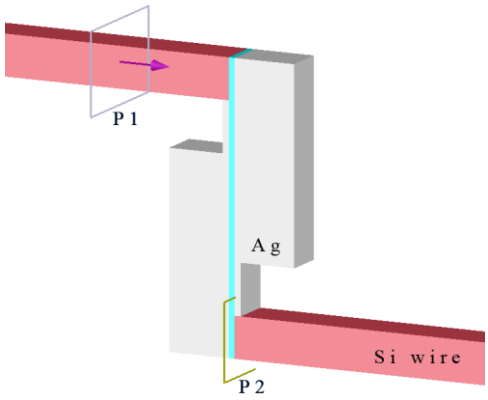

Fig. 9. Platform for in and out coupling from the PSW. The Si waveguide on the left will carry the signal to the orthogonally placed PSW. The light travels through the PSW and is again orthogonally coupled out into the output silicon waveguide. The overlay boxes indicate positions of the source and detector in the 3D FDTD simulations.

for the smoothed-out resonance peaks is because the orthogonal platform lacks a precisely defined cavity as the coupling occurs over a region along the PSW length. Of course including a tapering section in the parallel coupling scheme should be able to reduce the renounce effect. However, this taper increases the size of the structure and its complexity and may also increase the losses. Thus, it is obvious that the main advantage of the orthogonal coupling scheme is to obtain smooth and good coupling efficiency over wideband without the need for any matching stub or tapered section.

#136455 - $15.00 USD Received 11 Oct 2010; revised 22 Nov 2010; accepted 26 Nov 2010; published 8 Dec 2010

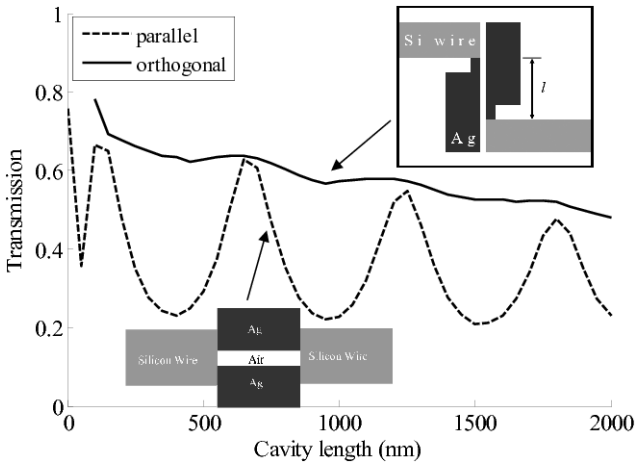

Fig. 10. Resonance effects are compared for the parallel and orthogonal configurations using results from 2D FDTD simulations. The inset indicates the cavity definition in the orthogonal configuration.

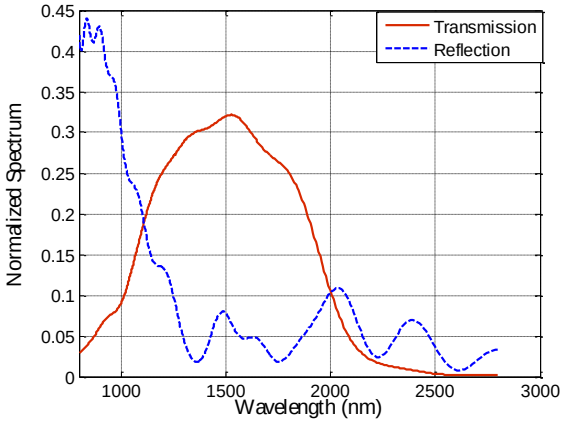

Fig. 11. The normalized transmission and reflection characteristics of the double coupler scheme shown in Fig. 9.

To accurately characterize the proposed configuration, 3D FDTD simulation has been performed for the configuration shown in Fig. 9. In this configuration two coupling junctions are included. The length of the plasmonic slot is 1.2 μm. The ratio of the transmitted power to the total input power is calculated and shown in Fig. 11 as the transmission spectrum. The peak of the transmission is calculated to be 0.322. The insertion loss of this double junction includes the coupling loss, in this case it is the square of the coupling loss of one junction, and the propagation loss. According to the modal calculations the loss of this junction is ~34.3%. By using this loss value along with the coupling values of one junction, the total insertion loss is calculated to produce a normalized transmission of 0.33, which is in good agreement with the FDTD results. The ratio of the reflected power to the total power is also calculated and shown in Fig. 11. It is clear that the reflected power around the operating wavelength range is insignificant.

#136455 - $15.00 USD Received 11 Oct 2010; revised 22 Nov 2010; accepted 26 Nov 2010; published 8 Dec 2010

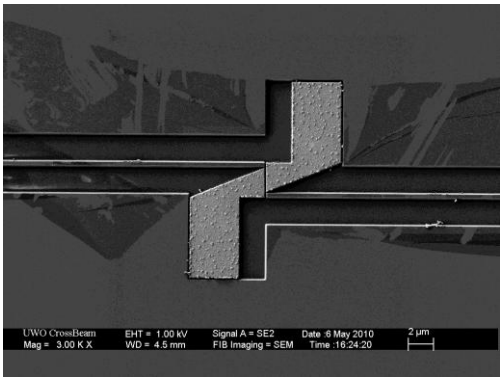

Fig. 12. Scanning electron microscope (SEM) picture for the orthogonal coupling scheme.

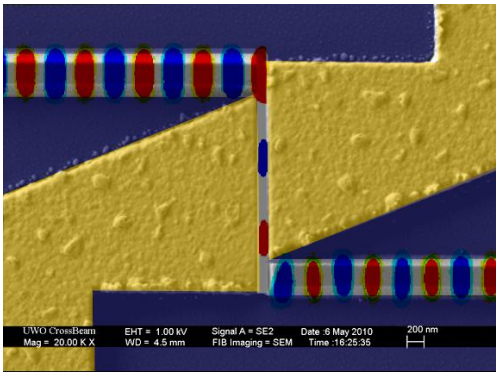

Fig. 13. Optical field propagation from Si waveguide through the PSW using FDTD simulation imposed on the SEM pic .

4. Fabrication and measurements

A SOI substrate with a 340 nm thick Silicon top layer and a 1 μm oxide layer is used to create the coupling platform. In the first step, alignment markers are patterned using electron beam lithography (EBL) followed by Au marker deposition and lift-off. Then Si waveguides with input and output tapers are patterned with EBL and etched using reactive ion etching (RIE). The Au markers are necessary for proper alignment of the waveguide to avoid any misalignment loss. The 2.5 μm to 400 nm wide tapers are each 2 mm long to ensure adiabatic mode compression and expansion.

After etching, the Si waveguides are 340 nm in height with a 400 nm nominal width after tapering. After patterning the Si waveguide layer, another EBL step is carried out and a window is opened for Ag deposition. Focused ion beam (FIB) is used to make the 50 nm wide slot across the 340 nm thick Ag film, creating the PSW directly adjacent to the Si waveguides as shown in Fig. 12. The simulated optical field inside the whole structure from the input silicon waveguide to the output one through the plasmonic slot region using FDTD at 1550 nm is shown in Fig. 13. Using electron beam lithography, in conjunction with FIB, the misalignment error is anticipated to be in the order of ~10-20 nm after fabrication optimization. This reduces the significance of the misalignment losses compared with other sources of losses such as propagation losses. The loss from this misalignment is not trivial to quantify in practice however.

#136455 - $15.00 USD Received 11 Oct 2010; revised 22 Nov 2010; accepted 26 Nov 2010; published 8 Dec 2010

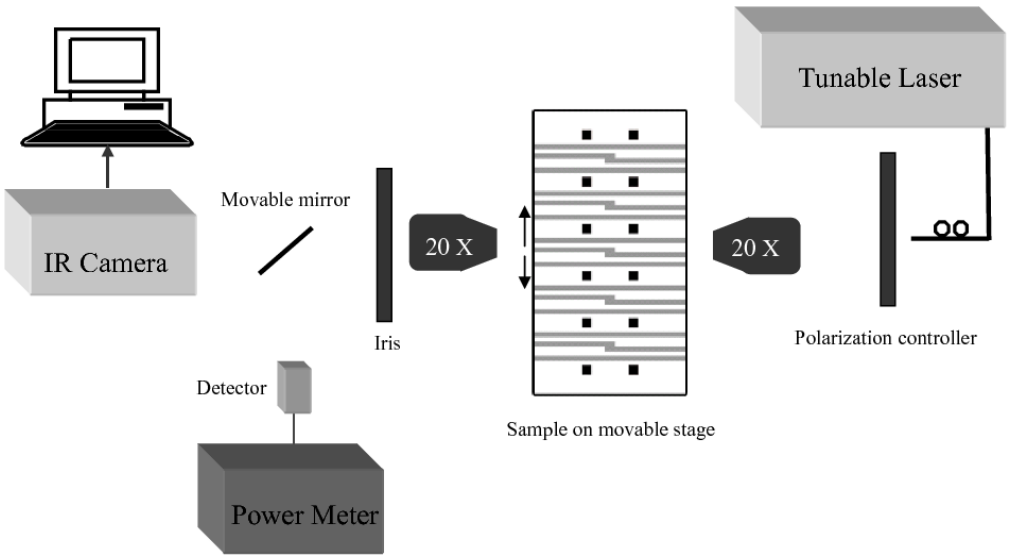

Fig. 14. Schematic diagram of the measurement setup.

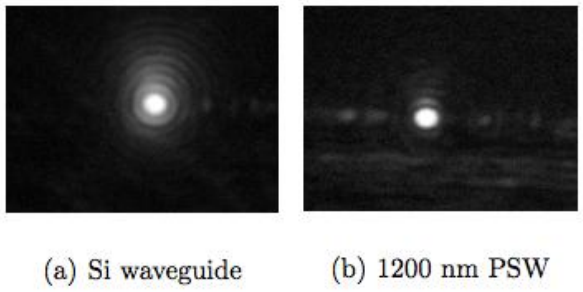

Fig. 15. Infrared camera images of the mode profile of Si waveguide after passing through PSW of 1200 nm length.

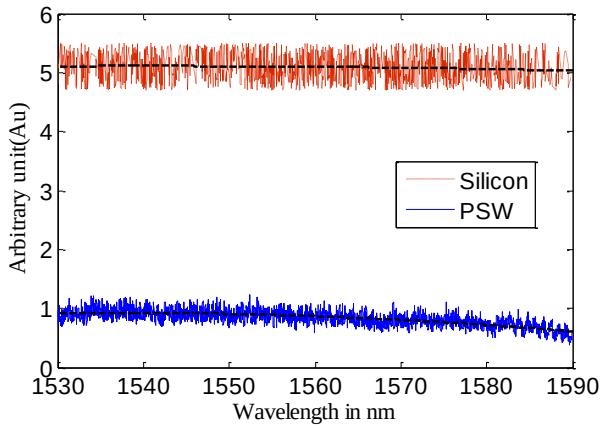

Fig. 16. The measured transmission characteristics for PSW with slot length of 1.2 μm and straight silicon waveguide with slot, the dashed lines represent the average results.

#136455 - $15.00 USD Received 11 Oct 2010; revised 22 Nov 2010; accepted 26 Nov 2010; published 8 Dec 2010

For measurements, a tunable laser source around 1560 nm is utilized. The light is focused onto the input silicon waveguide using a 20x objective lens and a similar lens is used to collimate the light at the output. The experimental setup is also shown in Fig. 14. An infrared camera image of the output Si waveguide mode after passing through a 1200 nm long PSW is shown in Fig. 15 with a reference sample where a straight Si waveguide without the plasmonic section is imaged. The transmission characteristics of a PSW of length 1200 nm are obtained over a 60 nm bandwidth centered around 1560 nm. The obtained results are also compared with those of the straight Si waveguide, as shown in Fig. 16. It is clear from this figure that the response of the proposed coupling scheme is flat over the measured bandwidth, with more than 18% of the Si waveguide power coupled through the PSW.

In general, the insertion loss of the PSW can be obtained using the following expression,

$$IL = L_{C1} + L_{pSi} + L_{pPSW} + L_{C2} + L_{C3} + L_{C4} \quad (1)$$

where L_{C1}, L_{C4} are the free space coupling losses to and from silicon waveguide, respectively. In addition, L_{pSi} and L_{pPSW} are the propagation losses in the silicon waveguide and PSW, respectively. Also L_{C2}, L_{C3} are the coupling losses between the PSW and silicon waveguide.

Using the reference measurements the L_{C1}, L_{C4} combined are measured to be 12.04 dB. L_{pSi} is also calculated using linear loss measurements to be ~5.64 dB/cm. The coupling loss L_{C2}, L_{C3} are obtained from FDTD using a coupling efficiency of 0.7x0.7 = 0.49.

The measurement results have also been utilized to calculate the propagation losses L_{pPSW}. The power transmission for a Si waveguide with the PSW waveguide inserted in it was measured to be 18% in comparison to the power transmission measured for straight-through Si waveguide. The difference in transmission between both can be attributed to the power lost in the PSW couplers as well as the propagation loss through the PSW.

According to this measurement, the coupling and PSW propagation losses are 7.45 dB. This is the main results of this experimental measurement, which is the total insertion loss of the PSW. If we assume that the coupling efficiency of the PSW and Si waveguide is 0.7 as obtained from FDTD, the propagation loss can be estimated to be ~4.35 dB. This is mainly due to metal loss, surface roughness, scattering, leakage due to misalignments.

This measured loss is higher than what obtained from simulation (1.8 dB). The difference is mainly due to the higher propagation loss and other sources of losses including misalignment, surface roughness, and scattering losses. This is mainly due to metal loss, surface roughness, scattering, leakage due to misalignments.

5. Conclusion

A novel coupling scheme between 400 nm wide silicon waveguides and a plasmonic slot waveguide of 50 nm width is proposed. An orthogonal junction design has been introduced to achieve the efficient wideband coupling and reduced resonances created by momentum mismatch between the sections. Since the momentum matching occurs naturally as a result of the orthogonal configuration, no tapering to the PSW or high-index filling of the plasmonic slot is necessary. These features allow for a much more flexible platform for sensing and interconnect prototyping applications. The orthogonal coupling scheme is studied analytically with momentum matching analysis that is in good agreement with FDTD simulated results, and the experimental results have been very promising.

#136455 - $15.00 USD Received 11 Oct 2010; revised 22 Nov 2010; accepted 26 Nov 2010; published 8 Dec 2010